ac susceptibility of high-temperature superconductors

M. J. Qin and X. X. Yao

Department of Physics and National Laboratory of Solid State Microstructures, Nanjing University, Center for Advanced Studies in Science and Technology of Microstructures, Nanjing 210093, People's Republic of China

(Received 20 November 1995; revised manuscript received 11 April 1996)

By numerically solving the flux creep equation, we have investigated the temporal and spatial evolution of the field profiles in a high-temperature superconducting slab immersed in an ac magnetic field together with a dc bias magnetic field, for the situation where the flux creep activation barrier U depends explicitly on current density j as $U(j)=(U_0/\mu)[(j_c/j)^{\mu}-1]$. The fundamental ac susceptibilities of the slab as a function of temperature for different dc bias magnetic fields B_d, ac magnetic field amplitudes $B_{\rm ac}$, and frequencies f have been derived in a unified picture, which reproduce many of the features exhibited by experiments. We have shown that the frequency-independent critical-state model breaks down in explaining these results, which however, can be well described by means of flux creep. We have also shown that part of the loss in the high-temperature superconductors is due to flux creep. [S0163-1829(96)07933-7]

I. INTRODUCTION

Magnetic measurements using alternating fields have long been recognized as an important tool in the verification of models for pinning and motion of vortices in the mixed state of type-II superconductors.[1–4] The complex ac susceptibility ($\chi_n=\chi_n'-i\chi_n''$) of the high-temperature superconductors in connection with flux motion has also attracted much attention in literature.[5–12] It has been well known that a measurement of the fundamental ac susceptibility ($\chi_1=\chi_1'-i\chi_1''$, denoted as $\chi=\chi'-i\chi''$ in the following) of the high-temperature superconductors as a function of temperature typically shows, just below the critical temperature T_c, a sharp decrease in the real part of the susceptibility χ', a consequence of diamagnetic shielding, and a peak in the imaginary part of the susceptibility χ'', representing losses. Also, $\chi'(T)$ and $\chi''(T)$ curves have been found to depend on the dc magnetic field, on the frequency of the ac magnetic field, and on the ac field amplitude. However, the physical model to calculate the real part χ' and the imaginary part χ'' still remains controversial at present. Among the proposed interpretations, the critical state model[2,13] may be the most used one for explaining the temperature-dependent characteristics of χ' and χ'' up to date, especially the Anderson-Kim model,[13] which is probably most used for comparison with experimental data in terms of the temperature and field dependence of critical current density $j_c(T,B)$.[14–18] However, it should be noted that although the critical-state model has successfully explained a broad range of experimental results, as a static hysteretic model, it is incapable of explaining the frequency-dependent ac susceptibility of the high-temperature superconductors. Unfortunately, frequency may be the most important variable in the study of vortex dynamics using ac susceptibility measurements.

Furthermore, it has been pointed out[19] that for the use of the critical-state model, the following conditions should be satisfied: (1) the sample is homogeneous and isotropic; (2) the sample has dimensions consistent with the model; (3) the field at which magnetization M is taken should be large enough such that j_c is not a strong function of the field; (4) flux lines are well pinned, that is, there is no flux creep. In the high-temperature superconductors at low temperature, this is generally true; (5) there is little contribution from surface barrier and reversible magnetization. Obviously, in ac susceptibility measurements, all these conditions for use of the critical-state model are seldom satisfied simultaneously, especially at high temperature which is mostly the case in ac susceptibility measurements and at low frequency, the flux creep effects cannot be ignored. Moreover, the frequency effects on the ac susceptibility can also be explained by flux creep.

The response of the high-temperature superconductors to the ac magnetic field can be either a linear one or a nonlinear one. The response of the system to the ac magnetic field is always linear at small enough ac field amplitude, which has been extensively studied in Refs. 20–22. In the vortex liquid state, the linear response regime can be divided into three different frequency regimes.[21] At high frequency, the response is characteristic of viscous motion of the vortex lattice (flux-flow regime) and one can neglect the pinning potential. At smaller frequencies, the ac response is carried by reversible vortex oscillations near their equilibrium positions (Campbell regime),[4] in this case, the ac response is essentially London-like: The sample behaves like a true superconductor, but with a larger penetration depth.[21] In the region of extremely low frequency, thermally activated vortex jumps between most favorable metastable states of the vortex lattice come into play (TAFF regime) and contribute to the ac response.

The linear response in the TAFF regime, as shown in Refs. 20–22, results from an Ohmic resistive state $E=\rho j$ in the sample, where $\rho(T,H)$, independent of j, is the thermally activated flux-flow resistivity. Therefore, the electrodynamics of a high-temperature superconductor in the TAFF regime where $E=\rho j$ is valid is nothing but the electrodynamics of a normal metal, albeit with an exponentially small resistivity ρ.[20] It is well known that the electrodynamics of a normal metal in an ac field is governed by the skin effect. Accordingly, the ac susceptibility of a high-temperature superconductor in the TAFF regime can be easily obtained as[20]

$$4\pi\chi' = \frac{1}{u}\frac{\sinh(u)+\sin(u)}{\cosh(u)+\cos(u)} - 1,$$

$$4\pi\chi'' = \frac{1}{u}\frac{\sinh(u)-\sin(u)}{\cosh(u)+\cos(u)}, \tag{1}$$

where $u = d/\delta_s = [(\omega/\rho)(2\pi d^2/c^2)]^{1/2}$, $\delta_s = (\rho c^2/2\pi\omega)^{1/2}$ is the skin depth, ω is angular frequency of the ac field, d is the thickness of the superconducting slab, and c is the velocity of light.

In the opposite case of a large ac field amplitude where the response of the system is highly nonlinear, the sample is taken through a complete hysteresis loop at a rate $\dot{B} = \omega B_{\rm ac}\cos(\omega t)$. A similar situation can be found in dc magnetization measurements where the sample responds to a field ramp at a constant rate of $\dot{H}$. The changing magnitude of the magnetic field at the surface results in an electric field gradient, which in turn induces a shielding current of magnitude $j < j_c$ in the sample interior. The spatial variation of j is determined by the actual form of the activation energy $U(j)$. If $U(j)$ is a strong nonlinear function of j, the current density remains constant within a shell of thickness $x_B = H_{\rm ac}/j$. The flux density profile in the region of penetration can thus be approximated by a straight line. The magnitude of j depends on the magnitude of the local electric field and therefore on the field sweep rate $\dot{H}$, and is given implicitly by the relation

$$U[j(\dot{H})] = k_B T \ln\left[\frac{\rho_0 j}{\mu_0 \dot{H} x_B}\right] \tag{2}$$

and the resistivity ρ can be written as

$$\rho = \rho_0 \exp\left[-\frac{U(j)}{k_B T}\right]. \tag{3}$$

The ac susceptibility measurement just corresponds to periodically ramping the field up and down between the values $B_d \pm B_{\rm ac}$ at the rate $\dot{B} \approx \omega B_{\rm ac}$. The current density should therefore behave in the same way as in the field ramp experiment. In the case of strong nonlinearity, the current density at $\omega t = \pi/2$ is constant over a surface shell of thickness $x_B = H_{\rm ac}/j$. The thickness x_B is actually the Bean ac penetration length, but with j_c replaced by $j(\omega)$. With the replacement $\dot{H} \rightarrow \omega H_{\rm ac}$ in Eq. (2), van der Beek *et al.*[21] derived

$$U[j(\omega)] = k_B T \ln\left[\frac{1}{\omega t_0}\right], \tag{4}$$

where the relaxation time $t_0 = \mu_0 H_{\rm ac}^2/\rho_0 j^2(\omega)$. Therefore, in the analysis of van der Beek *et al.*,[21] the important point is that the straight-line approximation provides a good description of the field profile inside the sample, thus their discussion proceeds along the same lines as the Bean analysis of the critical state, except that the screening current density instead of being the critical current density j_c now is reduced to $j(\omega)$ depending on the frequency due to creep. However, whether the straight-line approximation can be used or to what extent it can be used is still an open question.

Besides, other loss mechanisms, such as the superconductor glass model[23] and vortex lattice viscosity and viscous damping[24] are also presented. Therefore, further investigations are needed in order to elucidate the loss mechanism in the high-temperature superconductors.

Usually, in the critical-state model, it is more convenient to present χ' and χ'' as a function of the temperature-dependent penetration depth,[17] rather than as a function of the temperature, especially when the Anderson-Kim model, in which the flux density profile inside the sample is not a straight line, is invoked. Furthermore, the critical-state model cannot account for the observed increase of T_p, the temperature corresponding to the χ'' peak, with the frequency of the ac field. Effects of frequency on the ac response have also been analyzed by Müller,[14] he explained the frequency dependence on the basis of the critical-state model, taking into account the flux-creep effect. However, the results are not conclusive, because $\chi'(T)$ and $\chi''(T)$ for different frequencies have not been presented, and the assumption that $\nu = \eta f$ (η is a factor of 10^3–10^5, f is the frequency of the ac field) is not convincing. On the other hand, although expressions for χ' and χ'' have been derived in the linear response regime, to our best knowledge, no theoretical $\chi'(T)$ and $\chi''(T)$ curves have been presented in the nonlinear response regime, especially in a unified picture up to date. The present paper attempts to take all these points into account by starting from the flux-creep equation.

This paper is organized as follows. In Sec. II, we formulate the flux-creep problem in terms of a partial difference equation. This equation serves as a basis for our numerical calculation discussed in Sec. III. By using the numerical results, we discuss in Sec. IV the following: (1) The features of the flux and current density profiles inside the sample, according to which we will show that the straight-line approximation for the field profiles inside the sample works well through most of the sample region, (2) $\chi'(T)$ and $\chi''(T)$ curves at different dc bias magnetic fields, frequencies and ac field amplitudes, which reproduce many experimental observations in ac susceptibility measurements. The discussions of the ac loss mechanism in the high-temperature superconductors will be presented in Sec. V. Finally, Sec. VI is attributed to a summary of this work.

II. THE FLUX-CREEP EQUATION

The flux-creep equation, which governs the penetrating process of the flux from two surfaces into the sample can be obtained as follows. Since the electric field induced by the flux motion is $\mathbf{E} = \mathbf{B} \times \mathbf{v}$, by using the Maxwell equation $\nabla \times \mathbf{E} = -\partial \mathbf{B}/\partial t$, one obtains the equation describing flux motion

$$\nabla \times (\mathbf{B} \times \mathbf{v}) = -\frac{\partial \mathbf{B}}{\partial t}. \tag{5}$$

Generally, for the study of flux motion, one starts with the one-dimensional case: considering a slab geometry with the sample to be located between the planes $x = -d$ and $x = d$, and the external field $\mathbf{B} \| z$ parallel to the surface of the sample. Then Eq. (5) is reduced to

$$\frac{\partial B}{\partial t} = -\frac{\partial}{\partial x}(Bv). \tag{6}$$

The thermally activated flux velocity v is given by $v=v_0(j/j_c)\exp[-U(j)/k_BT]$, where $v_0=u\omega_m$, u is the hopping distance, ω_m is the microscopic attempt frequency, and the factor j/j_c is introduced to provide a gradual crossover to the viscous flow regime $v\propto j$ at $k_BT\gg U(j)$. The emphasis will be on the current density j-dependent activation energy U, showing the divergence for $j\to 0$, characteristic of the vortex-glass–collective-creep models,[25,26] namely $U(j)=(U_0/\mu)[(j_c/j)^{\mu}-1]$. The commonly used logarithmic dependence $U(j)=U_0\ln(j_c/j)$ and linear dependence $U(j)=U_0(1-j/j_c)$ will be considered elsewhere. The solution of the nonlinear flux-creep equation constitutes an intricate task even for the linear Anderson-Kim-type dependence $U(j)=U_0(1-j/j_c)$ if attempted analytically. Therefore, in the following, we will present numerical solutions of the flux-creep equation and the results will be compared with the experimental data presented in the literatures.

III. METHOD FOR NUMERICAL CALCULATION

Because of the symmetry of the problem, only the region $x\geqslant 0$ is considered. Then the boundary conditions are $B(x=d,t)=B_d+B_{\rm ac}\sin(2\pi ft)$ and $(\partial B/\partial x)(x=0,t)=0$, where B_d is the applied dc bias magnetic field, $B_{\rm ac}$ is the ac magnetic field amplitude, and f is the frequency of the ac magnetic field. The initial condition is $B(x,t=0)=B_d$. We must mention here that the present calculation, like those in the literature, is for a homogeneous hard superconductor with $H_{\rm cl}=0$. By introducing dimensionless variables

$$b=\frac{B}{B_d},\quad J=\frac{j}{j_c},\quad \tilde{x}=\frac{x}{d_0},\quad \hat{t}=f_0t,\quad b_{\rm ac}=\frac{B_{\rm ac}}{B_d},\qquad (7)$$

where d_0 and f_0 is the space and time scale, respectively. By using the Maxwell equation

$$\frac{\partial b}{\partial\tilde{x}}=-\frac{\mu_0j_cd_0}{B_d}J,$$

one gets

$$\frac{\partial b}{\partial t}-C\frac{\partial}{\partial x}\left\{b\frac{\partial b}{\partial x}\exp\left[-\frac{\sigma}{\mu}\left(-\frac{B_d}{\mu_0j_cd_0}\frac{\partial b}{\partial x}\right)^{-\mu}\right]\right\}=0,$$

$$b\left(x=\frac{d}{d_0},t\right)=1+b_{\rm ac}\sin(2\pi ft),$$

$$\frac{\partial b}{\partial x}(x=0,t)=0,$$

$$b(x,t=0)=1,\qquad (8)$$

where $\sigma=U_0(T,H)/k_BT$ and $C=[V_0\exp(\sigma/\mu)/f_0d_0](B_d/\mu_0j_cd_0)$. In Eq. (8), we have omitted the tildes over the dimensionless coordinate and time variables $\tilde{x}$ and $\tilde{t}$.

The numerical integration of Eq. (8) is carried out by using a simple single-step method. The discrete version of Eq. (8) is

$$b(x,t+\delta t)=b(x,t)+\frac{c\,\delta t}{2\delta x}\left\{b(x+\delta x,t)\frac{b(x+2\delta x,t)-b(x,t)}{2\delta x}\exp\left[-\frac{\sigma}{\mu}\left(-\frac{B_d}{\mu_0j_cd_0}\frac{b(x+2\delta x,t)-b(x,t)}{2\delta x}\right)^{-\mu}\right]\right.$$
$$\left.-b(x-\delta x,t)\frac{b(x,t)-b(x-2\delta x,t)}{2\delta x}\exp\left[-\frac{\sigma}{\mu}\left(-\frac{B_d}{\mu_0j_cd_0}\frac{b(x,t)-b(x-2\delta,t)}{2\delta x}\right)^{-\mu}\right]\right\}.\qquad (9)$$

The space step is chosen to be $\delta x=4$, and the time step δt depends on the physical parameters used in Eq. (9).

For obtaining the ac susceptibility, we have to calculate the magnetization M for the applied time-dependent field $B(t)=B_d+B_{\rm ac}\sin(2\pi ft)$. For the geometry considered, the magnetization is given by

$$\mu_0M(t)=\frac{B_d}{d/d_0}\int_0^{d/d_0}b(x)dx-[B_d+B_{\rm ac}\sin(2\pi ft)]\qquad (10)$$

and the complex ac susceptibility $\chi_n=\chi_n'-i\chi_n''$, where

$$\chi_n'=\frac{1}{\pi B_{\rm ac}}\int_0^{2\pi}\mu_0M(t)\sin(n\omega t)d(\omega t),$$
$$\chi_n''=\frac{1}{\pi B_{\rm ac}}\int_0^{2\pi}\mu_0M(t)\cos(n\omega t)d(\omega t),\qquad (11)$$

can be easily derived by means of fast Fourier transform (FFT). And the fundamental ac susceptibility χ_1' and χ_1'' (denoted as χ' and χ'' in this paper) has clear physical meaning, the real part χ' corresponds to the dispersive magnetic response and the imaginary part χ'' corresponds to energy dissipation.

Before calculating Eq. (9) numerically, we have to present the parameters used in Eq. (9), among which the temperature and field dependence of the critical current density $j_c(T,H)$ and the apparent activation energy $U_0(T,H)$ must be presented, in order to account for the temperature and field dependence of the ac susceptibility. As for the temperature dependence, we chose the following forms:

$$j_c(T,B=0)=j_{c0}(1+t^2)^{-1/2}(1-t^2)^{5/2},$$
$$U_0(T,B=0)=U_{00}(1-t^4),\qquad (12)$$

which are the prediction for a single vortex results.[27] In Eq. (12), t is the reduced temperature $t=T/T_c$, and T_c is the critical temperature of the sample.

As for the field dependence, we chose the form

$$j_c(T=0,B)=j_{c0}\frac{B_0}{B_0+|B|} \tag{13}$$

as suggested by Kim, Hempstead, and Strnad.[28] Usually, the field dependence of U_0 takes the form $U_0(B)\propto 1/|B|$. In this work, in order to avoid introducing another parameter and for simplicity, we chose the field dependence of U_0 to be the same as that of j_c

$$U_0(T=0,B)=U_{00}\frac{B_0}{B_0+|B|}. \tag{14}$$

Taking Eqs. (12)–(14) into account, we have

$$j_c(T,B)=j_{c0}(1+t^2)^{-1/2}(1-t^2)^{5/2}\frac{B_0}{|B|+B_0},$$

$$U_0(T,B)=U_{00}(1-t^4)\frac{B_0}{|B|+B_0}, \tag{15}$$

and the parameters j_{c0}, U_{00}, and B_0 are independent of T and B. It must be stressed here that the above form is taken only because of analytical simplicity and not because it is expected to represent the actual behavior of the high-temperature superconductors. The actual temperature and field dependence of the critical current density and the apparent activation energy can be determined by best fitting the numerically calculated $\chi'(T)$ and $\chi''(T)$ curves with specific form of $j_c(T,B)$ and $U_0(T,B)$ to the experimental data.

The order of magnitude of $v_0=u\omega_m$ can be estimated by noting that when $j=j_c$, the relevant activation energy $U(j_c)=0$ and a flux-flow state is established. The corresponding electric field is then $E=u\omega_m B=j_c\rho_f$, where the flux-flow resistivity $\rho_f\approx\rho_n B/B_{c2}$ according to the Bardeen-Stephen theory of flux flow.[29] We thus approximately obtain $u\omega_m=j_c\rho_n/B_{c2}$ where ρ_n is the normal-state resistivity and B_{c2} is the upper critical field. With $j_c=10^9$ A/m^2, $\rho_n=5\times10^{-7}$ Ωm, and $B_{c2}=100$ T, one finds $u\omega_m\approx5$ m/s. For all examples calculated in this work, we shall arbitrarily take $u\omega_m=1$ m/s. The values for other parameters used in Eq. (8) are $j_{c0}=10^{11}$ A/m^2, $f_0=10$ Hz, $d_0=10^{-6}$ m, $d=10^{-4}$ m, $U_{00}/k_BT_c=10$, $B_0=1$ T.

As for the important exponent μ in $U(j)=(U_0/\mu)[(j_c/j)^{\mu}-1]$, characteristic of the vortex-glass–collective-pinning models,[25,26] the vortex-glass theory has no prediction for its field and temperature dependence. Rather, it is regarded as a universal exponent with value $\mu\leqslant1$. However, in a theoretical treatment of collective pinning, Feigel'man *et al.*[26] predicted the existence of three different regimes of current density j: $j\ll j_c$, $\mu=7/9$; $j<j_c$, $\mu=3/2$; and $j\sim j_c$, $\mu=1/7$. Experimentally, μ has also been found to depend on both temperature and field.[30] However, a single value of μ can also well describe the experimental data for a wide range of current densities in many works.[31–33] Recently, by ac susceptibility measurements, a single value of $\mu=0.64$ has also been found for $TlSr_2Ca_2Cu_3O_y$.[34] Therefore, in this work, we choose a single value of $\mu=0.6$, independent of temperature and field, for the numerical calculation for simplicity.

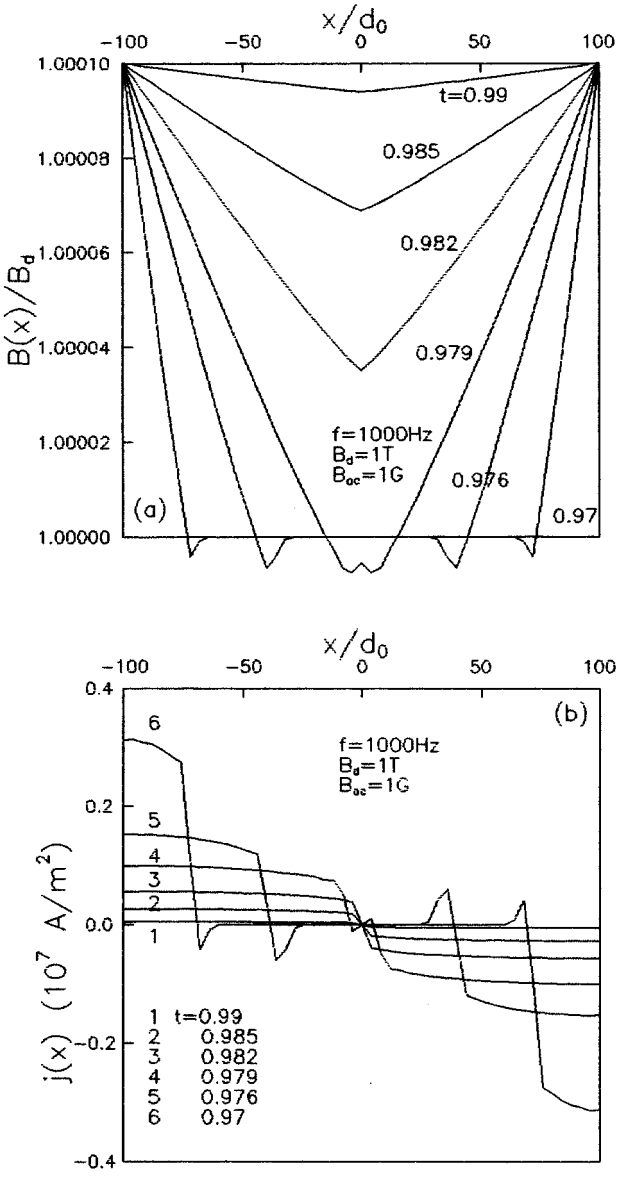

FIG. 1. (a) The flux density profiles in the slab at $B=B_d+B_{ac}$ ($\omega t=\pi/2$) for $f=1000$ Hz, $B_d=1$ T, and $B_{ac}=1$ G at various temperatures. (b) The corresponding current density profiles in the slab.

Equations and results are expressed in SI units. Volume susceptibility is dimensionless, with full diamagnetism corresponding to a susceptibility of -1.

IV. RESULTS AND DISCUSSIONS

In Figs. 1(a) and 1(b), we plot the flux and current density profiles at the moment $\omega t=\pi/2$ that the applied magnetic field reaches the maximum value $B(t)=B_d+B_{ac}$ and at various temperatures, for $f=1000$ Hz, $B_d=1$ T, and $B_{ac}=1$ G, respectively. With increasing temperature, the flux penetrates more quickly into the sample. And interestingly, both in the flux density profiles and in the current density profiles, there exist some spikes at relatively low temperatures, say, $t=0.97$, 0.976, and 0.979. At higher temperatures, however, the spikes disappear, see the curves at $t=0.982$, 0.985, and 0.99, which can be explained by the magnetic relaxation ef-

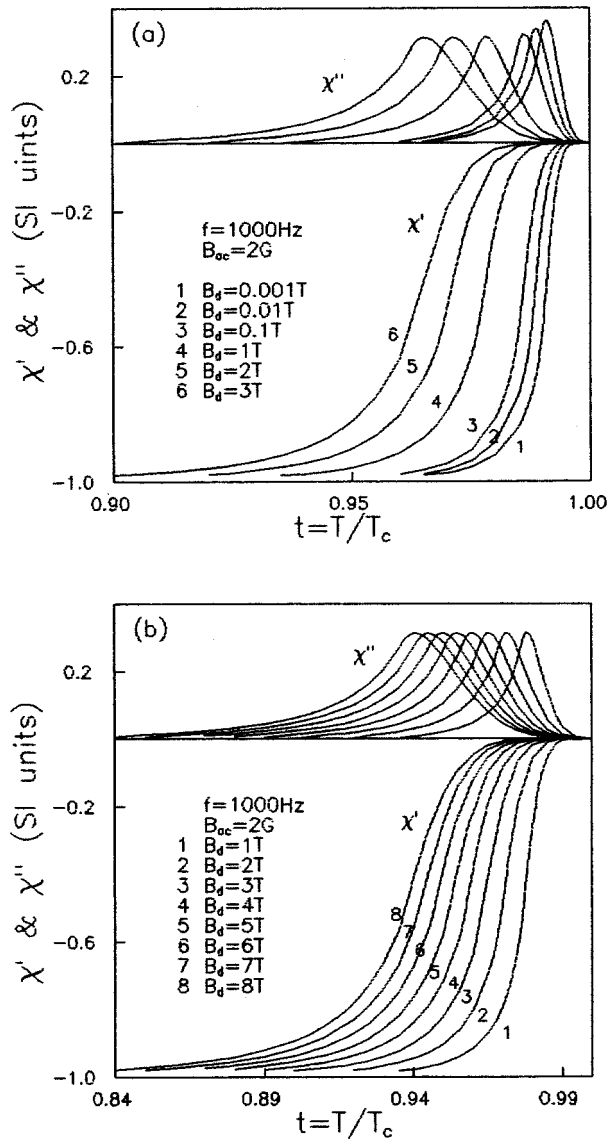

FIG. 2. (a) The calculated curves of χ' and χ'' as a function of temperature at various dc magnetic fields, for $f=1000$ Hz and $B_{\rm ac}=2$ G. (b) The same as (a) except at larger dc magnetic fields.

fect. Because the relaxation effect tends to decrease the magnetization, i.e., tends to decrease the slope of the flux density profile, and therefore, tends to eliminate the spikes. At high temperatures, the relaxation is so quick that the spikes disappear. Another direct result of flux creep is that at all temperatures, the current densities $j(T)$ are always smaller than the corresponding critical current densities $j_c(T)$. Therefore, in ac susceptibility measurements, flux creep should be considered.

The effect of the dc magnetic field on the ac susceptibility can be seen clearly from Fig. 2, where the calculated curves of χ' and χ'' as a function of temperature at various dc bias fields, for $f=1000$ Hz and $B_{\rm ac}=2$ G are plotted. As the dc field increases, the transition in $\chi'(T)$ and $\chi''(T)$ becomes broad, as can be seen in both $\chi'(T)$ and $\chi''(T)$ curves. The peak height in χ'' decreases appreciably with increasing dc field at a value of 3 T and below, see Fig. 2(a). These results are in good agreement with experimental data of Ishida and Goldfarb[17] and have also been modeled by Müller.[14] However, it can be seen from Fig. 2(b) as the dc field further increases, the peak height in χ'' remains constant up to 8 T. Experimentally, it has also been observed that with increasing dc fields, the peak height in χ'' increases to a certain value and remains constant for further increasing dc field.[18] This observation may indicate that instead of Eqs. (13) and (14), other forms of $j_c(B)$ and $U_0(B)$ should be taken into account.

In Fig. 3, we plot the calculated curves of χ' and χ'' as a function of temperature at various ac field amplitudes, for $f=1000$ Hz and $B_d=100$ G. As $B_{\rm ac}$ increases, the height and breadth of the peak in χ'' increases as it moves to lower temperature, which has been experimentally well known.[17] However, as the ac field amplitude further increases, the peak height in χ'' decreases slightly as shown in Fig. 3(b). This is understandable, considering that when the ac field and dc field are of the same order of magnitude, the ac field may have the same effect as that of the dc field, therefore, similar to those shown in Fig. 2(a), the peak height in χ'' should decrease with increasing ac field amplitude. It should be noted that the frequently used simplified Anderson-Kim critical-state model, in which the critical current density inversely depends on the field, does not explain the change in the peak height of χ'' with $B_{\rm ac}$ seen experimentally.[16] We explore the effect of the ac field amplitude further in Fig. 3(c) in which the calculated curves of χ' and χ'' as a function of temperature at various ac field amplitudes are plotted, for $f=1000$ Hz and $B_d=1$ T. The condition $B_d \gg B_{\rm ac}$ is satisfied. It can be seen from Fig. 3(c) that no changes in the peak height of χ'' are observed. This effect is similar to that of dc field at large B_d shown in Fig. 2(b).

The essential feature of the present calculation is that it can be used to study the frequency effect on the ac susceptibility. Shown in Fig. 4(a) are the flux density profiles at the moment $\omega t=\pi/2$ when the applied magnetic field reaches the maximum value $B=B_d+B_{\rm ac}$ at various frequencies, for $B_d=1$ T, $B_{\rm ac}=100$ G, and $t=0.935$. As the frequency decreases, the relaxation time for the magnetization to decay becomes longer, resulting in a smaller current density at low frequencies, which can be seen from the slope of the flux profiles in Fig. 4(a). Moreover, similar to Fig. 1(a), there also exist some spikes in the flux density profiles at high frequencies, which is the result of the relaxation effect as discussed in detail above.

We plot the calculated curves of χ' and χ'' as a function of temperature at various frequencies, for $B_d=1$ T and $B_{\rm ac}=100$ G in Fig. 4(b). As the frequency decreases, the transition temperature shifts to lower value, the peak height in χ'' decreases and the breadth in χ'' increases as it moves to lower temperature, which is in good agreement with experimental data.[12,18] It should be noted that the calculated result in Fig. 4 is conducted at constant B_d and $B_{\rm ac}$, therefore, it is independent of the chosen form of $j_c(B)$ and $U_0(B)$ and can be regarded as a universal behavior.

By now, we have presented ac susceptibility as a function of temperature for different dc fields B_d, ac field amplitudes $B_{\rm ac}$, and frequencies f in a unified picture, which is in good agreement with experimental data. In the following, we will show that flux creep can account for all these features.

When an ac magnetic field is applied to the sample surface, the sample is taken through a complete hysteresis loop

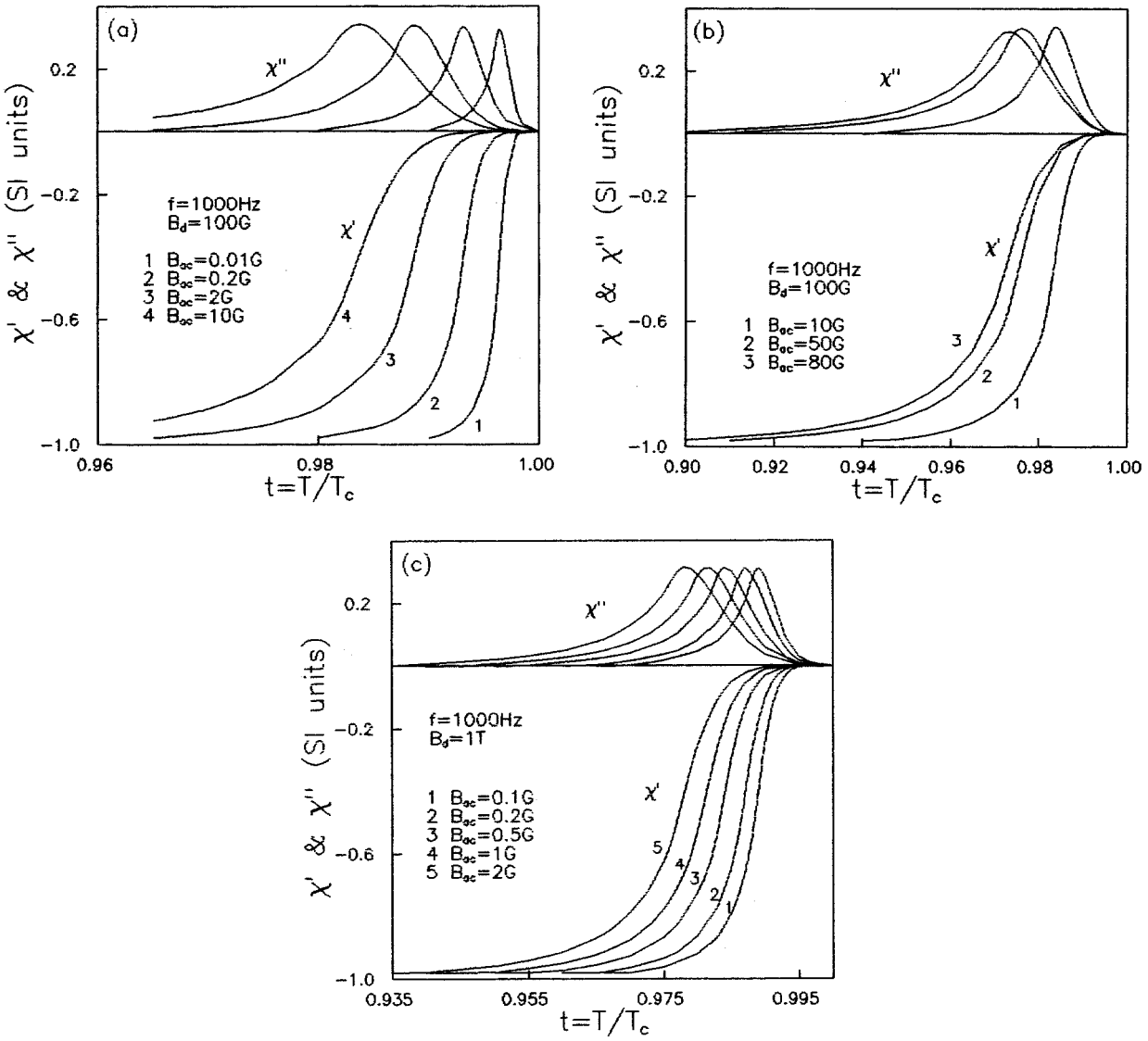

FIG. 3. (a) The calculated curves of χ' and χ'' as a function of temperature at various ac field amplitudes, for $f=1000$ Hz and $B_d=100$ G. (b) The same as (a) except at larger ac field amplitudes. (c) The same as (a) except at $B_d=1$ T.

within the time period $t=1/f$, where t instead of being the order of hours now is of the order of $\sim 10^{-5}$–10 s in this work. In this case, the decay of the critical state competes with the time scale imposed on the system by the external ac magnetic field. And the decay of the magnetization is cut on the time scale $t=1/f$ such that the screening currents flowing in the sample are given by Eq. (4):

$$U(j)=k_BT\ \ln\frac{1}{\omega t_0}. \tag{16}$$

The screening current density instead of being the critical current density, now is reduced to $j(\omega)=U^{-1}[k_BT\ \ln(1/\omega t_0)]$, and U^{-1} is the inverse function of $U(j)$.

Shown in Fig. 5 are the field profiles at $\omega t=\pi/2$ when the applied time-dependent field reaches the maximum value $B=B_d+B_{\rm ac}$ for various frequencies $f=0.1$, 1, 10, 100, 1000, 10 000, and 100 000 Hz, at temperature $t=t_p=T_p/T_c$, where χ'' attain the maximum values. It can be seen that although the frequency ranges from 0.1 to 100 000 Hz, the flux profiles at $t=t_p$ and $\omega t=\pi/2$ are almost the same, which superimposed each other except near the center of the sample. It can be seen from Fig. 4(a) that in order for different frequencies to attain the same situation shown in Fig. 5, a lower temperature is required to overcome the relaxation effect at low frequency, resulting in lower t_p, which is the case shown in Fig. 4(b). For the frequency ranges from 0.1 Hz to 100 000 Hz, the corresponding t_p changes from 0.924 to 0.96, respectively. In this case, the penetration depth d_p of the ac magnetic field is of the order of the half thickness of the slab, that is, $d_p\approx d$. And the straight-line approximation for the field profiles works well throughout most of the sample region, except near the center of the sample. Then the current density can be approximated by $j(\omega)=B_{\rm ac}/\mu_0 d$. From Eq. (16), we have

$$U\left(B,j=\frac{B_{\rm ac}}{\mu_0 d}\right)=k_BT\ \ln\frac{1}{\omega_{\rm peak}t_0}. \tag{17}$$

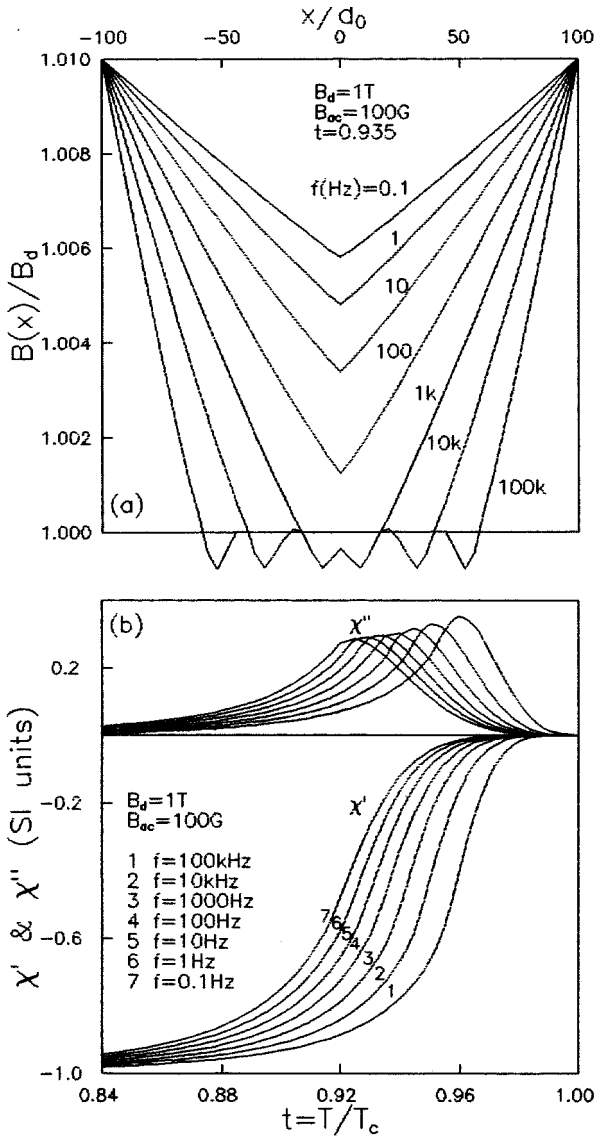

FIG. 4. (a) The flux density profiles in the slab at $B_d=1$ T, $B_{ac}=100$ G, and $t=0.935$, for various frequencies. (b) The calculated curves of χ' and χ'' as a function of temperature at various frequencies, for $B_d=1$ T and $B_{ac}=100$ G.

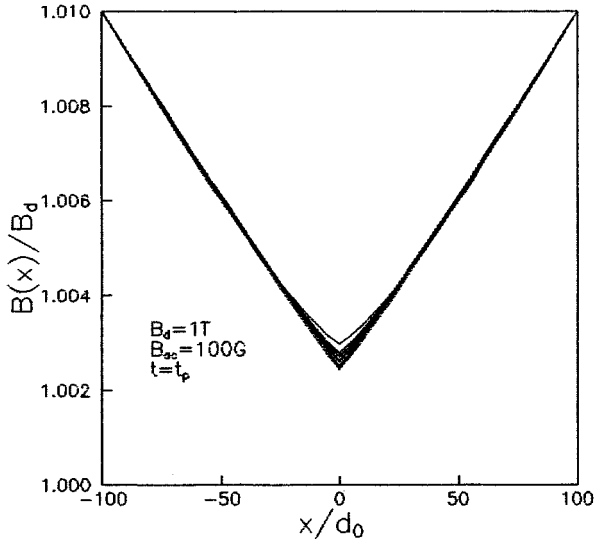

FIG. 5. The flux density profiles in the slab at $B=B_d+B_{ac}$ ($\omega t=\pi/2$) for various frequencies at $B_d=1$ T, $B_{ac}=100$ G, and at the temperature $t=t_p$ where χ'' attain the maximum values. $t_p=0.924$, 0.928, 0.933, 0.938, 0.944, 0.951, and 0.96 for $f=0.1$, 1, 10, 100, 1000, 10 000, and 100 000 Hz, respectively.

Thus the position of the peak in χ'' will strongly depend on the ac field amplitude B_{ac}, the dc field B_d, and the frequency f. With decreasing B_{ac} the activation energy is increased and the temperature where the dissipation peak occurs is shifted to higher values, which is the case shown in Fig. 3. Similarly, with decreasing B_d, the activation is also increased as can be seen from Eq. (15) and the temperature where the dissipation peak occurs is shifted to higher values, which is the case shown in Fig. 2. However, with decreasing frequency f, the activation energy is decreased as can be seen from Eq. (17) and the temperature where the dissipation peak occurs is shifted to lower values, which is the case shown in Fig. 4(b).

In order to study the process more carefully, we plot the field profiles and current density profiles in a period of the ac field, that is, at $\omega t=0$ or 2π ($B=B_d$), $\omega t=\pi/2$ ($B=B_d+B_{ac}$), $\omega t=\pi$ ($B=B_d$), and $\omega t=3\pi/2$ ($B=B_d-B_{ac}$), for $f=10$ Hz, $B_d=1$ T, $B_{ac}=1$ G, and $t=0.976$, in Figs. 6(a) and 6(b), respectively. As the field is ramped from B_d+B_{ac} to B_d ($\omega t=\pi/2$ to $\omega t=\pi$) at a sweep rate $\dot{B}=\omega B_{ac}\cos(\omega t)$, in the shell of the sample, on which the sweep rate has effect and the current density changes sign, the current density $|j|$ is larger at $\omega t=\pi$ than that at $\omega t=\pi/2$, because the sweep rate $|\dot{B}|=\omega B_{ac}$ at $\omega t=\pi$ is larger than $|\dot{B}|=0$ at $\omega t=\pi/2$. However, in the interior of the sample, on which the sweep rate has no effect, we see that the current density relaxes to a smaller value, clearly showing the relaxation effect. Similar phenomenon can also be seen when the field is swept from B_d-B_{ac} to B_d ($\omega t=3\pi/2$ to $\omega t=2\pi$ or 0). Moreover, at lower temperatures or at higher frequencies, where the relaxation is not so effective and the flux in the sample interior does not relax into the center of the sample, a spike is expected when the field is swept from B_d+B_{ac} to B_d-B_{ac} and *vice versa*, which is the case shown in Figs. 1(a) and 4(a).

From Figs. 1, 4, and 6, we can see that the straight-line approximation works well through most of the sample region. Although a minor correction may result from flux creep, the approximation remains valid as a zero-order approximation, especially at lower temperature and at high frequencies, where the relaxation rate is relatively slow.

It should be mentioned here that the linear response regime is not considered in the above calculation. The basic assumption on which the linear response relies is the finiteness of the activation barrier $U(j)$ in the small current density limit, $U(j\to 0)=U_0<\infty$. Such a behavior of the creep barriers is expected to be realized in the vortex liquid at high temperatures $T>T_g$, where T_g is the vortex-glass transition temperature. However, in this work, considering the success of the vortex-glass–collective-pinning model in describing magnetic relaxation experiments, we choose the activation barrier $U(j)=(U_0/\mu)[(j_c/j)^{\mu}-1]$. Such a barrier diverges as j goes to zero, therefore, the linear response regime is not expected. Fortunately, the linear response regime has been

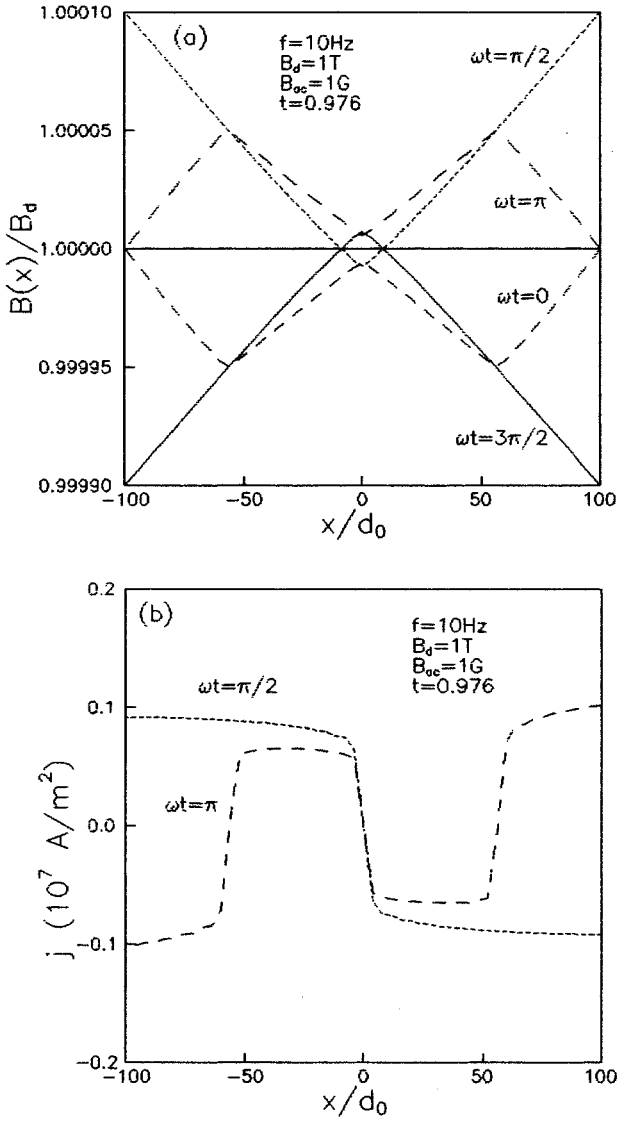

FIG. 6. (a) the flux density profiles in the slab at $\omega t=0$, $\omega t=\pi/2$, $\omega t=\pi$, and $\omega t=3\pi/2$, at $f=10$ Hz, $B_d=1$ T, $B_{\rm ac}=1$ G, and $t=0.976$. (b) The corresponding current density profiles in the slab.

understood relatively well, as discussed in detail in Sec. I. The linear response regime and the crossover from the linear response regime to the nonlinear response regime will be considered elsewhere.

V. THE LOSS MECHANISM

Because the hysteretic loss is proportional to the area of the magnetization loop, the peak in χ'' and the changes in the peak height of χ'' can be explained by considering the magnetization loops at different temperatures. In Fig. 7, we plot the magnetization loops at three temperatures $t=0.84$, $t=t_p=0.938$, and $t=0.99$, for $f=100$ Hz, $B_d=1$ T, and $B_{\rm ac}=100$ G. For $t<0.84$, the ac field causes the shielding currents to flow on the surface of the sample and a line to be traced out in the $M-B$ plane, which means there is no hysteresis and $\chi''=0$. For T somewhat below T_c, j_c has decreased and the shielding currents have to flow within the sample. The hysteresis loop in the $M-B$ plane has an area

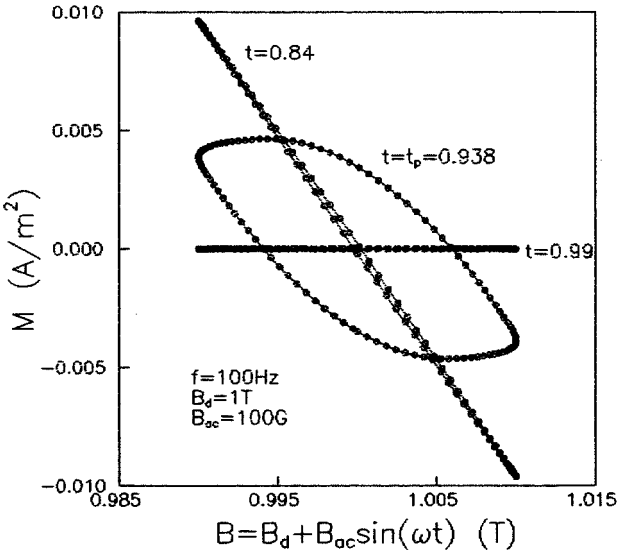

FIG. 7. The magnetization loops at $t=0.84$, $t=t_p=0.938$, and $t=0.99$, for $f=100$ Hz, $B_d=1$ T, and $B_{\rm ac}=100$ G.

associated with it and $\chi''>0$. The losses and χ'' attain their maximum values after supercurrents and penetrated flux reach the center of the sample at $t=t_p$, see Fig. 5. As T approaches T_c ($t=0.99$), j_c approaches 0, and the magnetization also goes to 0, the magnetization loop has collapsed, and there is no area to the loop and no hysteretic loss and $\chi''=0$. This interpretation is in accordance with the expectations of the critical state model, in which all energy losses are hysteretic and frequency independent.

However, the effect of frequency can be seen clearly from Fig. 8, where the magnetization loops at two frequencies $f=0.1$ and 100 000 Hz, for $B_d=1$ T, $B_{\rm ac}=100$ G, and $t=0.935$ are plotted. The area of the magnetization, which is proportional to the hysteretic loss, is larger at low frequency than that at high frequency. From Eq. (16), we can see that at

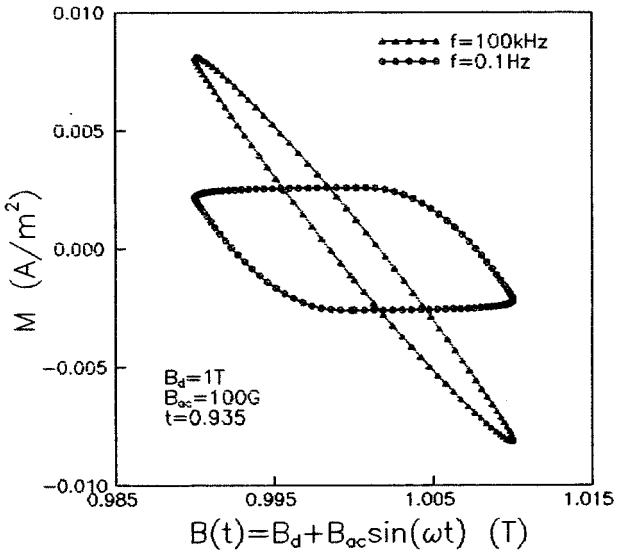

FIG. 8. The magnetization loops at $f=0.1$ and 100 000 Hz, for $B_d=1$ T, $B_{\rm ac}=100$ G, and $t=0.935$.

high enough frequency, $U \to 0$, the system is very close to the critical state, and flux creep can be ignored, then $j \approx j_c$. However, as the frequency decreases, $U(j)$ increases and the system decays away from the critical state and the current j decays to a value smaller than the critical current density, resulting in an increase of loss. Furthermore, at a low frequency, in order to attain the same situation as at a high frequency, a lower temperature is required to overcome the flux-creep effect, which can also account for the observed decrease of T_p, the temperature corresponding to the χ'' peak, with decreasing frequency of the ac magnetic field shown in Fig. 4(b).

VI. CONCLUSIONS

In conclusion, we have numerically solved the flux-creep equation for the case where a high-temperature superconducting slab is immersed in an ac magnetic field together with a dc bias magnetic field. The temporal and spatial evolution of the flux density profiles inside the sample and the magnetization loops have been obtained. The calculated curves of the fundamental ac susceptibility χ' and χ'' as a function of temperature for different dc magnetic fields, ac field amplitudes, and frequencies reproduce many of the features exhibited by experiments. We have shown that the frequency-independent critical-state model breaks down in explaining these results, which however, can be well described by means of flux creep and the straight-line approximation provides a good description of the field profiles inside the slab. We have also shown that the part of the loss in the high-temperature superconductors is due to flux creep.

ACKNOWLEDGMENT

This work was supported by Tianma Microelectronics Co. Ltd. in Shenzhen.

[1] Ph. Seng, R. Gross, U. Baier, M. Rupp, D. Koelle, R. P. Huebener, P. Schmitt, G. Saemann-Ischenko, and L. Schultz, Physica C **192**, 403 (1992).
[2] C. P. Bean, Rev. Mod. Phys. **2**, 31 (1964).
[3] J. I. Gittleman and B. Rosenblum, Phys. Rev. Lett. **16**, 734 (1991).
[4] A. M. Campbell, J. Phys. C **2**, 1492 (1969); **4**, 3186 (1971).
[5] A. P. Malozemoff, T. K. Worthington, Y. Yeshurun, F. Holtzberg, and P. H. Kes, Phys. Rev. B **38**, 7203 (1988).
[6] J. van den Berg, C. J. van der Beek, P. H. Kes, J. A. Mydosh, M. J. V. Menken, and A. A. Menovsky, Supercond. Sci. Technol. **1**, 242 (1989).
[7] A. Gupta, P. Esquinazi, H. F. Braun, and H. W. Neumüller, Europhys. Lett. **10**, 663 (1989).
[8] P. L. Gammel, J. Appl. Phys. **67**, 4676 (1990).
[9] J. H. P. M. Emmen, G. M. Stollman, and W. J. M. de Jonge, Physica C **169**, 418 (1990).
[10] J. H. P. M. Emmen, V. A. M. Brabers, and W. J. M. de Jonge, Physica C **176**, 137 (1991).
[11] C. J. van der Beek and P. H. Kes, Phys. Rev. B **43**, 13 032 (1991).
[12] F. Gömöry and T. Takács, Physica C **217**, 297 (1993).
[13] P. W. Anderson and Y. B. Kim, Rev. Mod. Phys. **36**, 39 (1964).
[14] K. H. Müller, Physica C **159**, 717 (1989); **168**, 585 (1990).
[15] J. R. Clem, Physica C **50**, 153 (1988).
[16] L. Ji, R. H. Sohn, G. C. Spalding, C. J. Lobb, and M. Tinkham, Phys. Rev. B **40**, 10 936 (1989).
[17] T. Ishida and R. B. Goldfarb, Phys. Rev. B **41**, 8937 (1990).
[18] C. Y. Lee and Y. H. Kao, Physica C **241**, 167 (1995).
[19] R. B. Goldfarb, M. Lelental, and C. A. Thompson, in *Magnetic Susceptibility of Superconductors and Other Spin Systems*, edited by R. A. Hein, T. L. Francavilla, and D. H. Liebenberg (Pienum, New York, 1991), p. 68.
[20] G. Blatter, M. N. Feigel'man, V. B. Geshkenbein, A. J. Larkin, and V. M. Vinokur, Rev. Mod. Phys. **66**, 1125 (1994).
[21] C. J. van der Beek, V. B. Geshkenbein, and V. M. Vinokur, Phys. Rev. B **48**, 3393 (1993).
[22] V. B. Geshkenbein, V. M. Vinokur, and R. Fehrenbacher, Phys. Rev. B **43**, 3748 (1989).
[23] A. Gianelli and C. Giovannella, Physica A **168**, 277 (1990).
[24] S. Takács, F. Gömöry, and P. Lobotka, IEEE Trans. Magn. **27**, 1057 (1991).
[25] M. P. A. Fisher, Phys. Rev. Lett. **62**, 1415 (1989); D. S. Fisher, M. P. A. Fisher, and D. A. Huse, Phys. Rev. B **43**, 130 (1991).
[26] M. V. Feigel'man, V. B. Gashkenbein, and A. I. Larkin, Physica C **167**, 177 (1990); M. V. Feigel'man, V. B. Geshkenbein, and V. M. Vinokur, Phys. Rev. B **43**, 6263 (1991).
[27] R. Griessen, H. H. Wen, A. J. J. van Dalen, B. Dam, J. Rector, H. G. Schnack, S. Libbrecht, E. Osquiguil, and Y. Bruynseraede, Phys. Rev. Lett. **72**, 1910 (1994).
[28] Y. B. Kim, C. F. Hempstead, and A. R. Strnad, Phys. Rev. Lett. **9**, 306 (1962).
[29] J. Bardeen and M. J. Stephen, Phys. Rev. **140**, 1197 (1965).
[30] Yang Ren Sun, J. R. Thompson, Y. J. Chen, D. K. Christen, and A. Goyal, Phys. Rev. B **47**, 14 481 (1993).
[31] Donglu Shi and S. Salem-Sugui, Jr., Phys. Rev. B **44**, 7647 (1991).
[32] H. L. Ji, Z. X. Shi, X. Jin, X. X. Yao, X. S. Rong, Y. M. Ni, and Z. X. Zhao, J. Appl. Phys. **75**, 1671 (1994).
[33] Y. Rui, H. L. Ji, X. N. Xu, H. M. Shao, M. J. Qin, X. Jin, X. X. Yao, X. S. Rong, B. Ying, and Z. X. Zhao, Phys. Rev. B **51**, 9161 (1995).
[34] S. Y. Ding, G. Q. Wang, X. X. Yao, H. T. Peng, Q. Y. Peng, and S. H. Zhou, Phys. Rev. B **51**, 9107 (1995).